Pionization: A method to study the nuclear surface

S. Wycech [*]
Theory Department, National Centre for Nuclear Research, Pasteura 7, 02-093 Warsaw, Poland

K. Piscichia [†]
Centro Ricerche Enrico Fermi – Museo Storico della Fisica e Centro Studi e Ricerche "Enrico Fermi", Via Panisperna, 89a, 00184 Roma RM, Italy
and Laboratori Nazionali di Frascati, INFN, Via Enrico Fermi, 54, 00044 Frascati RM, Italy

(Received 11 May 2023; accepted 25 May 2023; published 13 July 2023)

The nuclear absorption of antiprotons from atomic states is discussed. The formation of π mesons and measurements of mesonic charge distributions yield information on the structure of nuclear surface in particular on neutron skin thickness in some nuclei. Our purpose is to develop a procedure for analyzing the results of the PUMA experiment, envisaged to study the nuclear surface of unstable nuclei. The procedure is tested on old experiments in stable nuclei. The first step is to extract, from charge distributions, the parameters describing final state absorption and charge-exchange interactions of the mesons. In parallel, these parameters are calculated in terms of pion optical potentials. In this way one learns the atomic states from which the absorption happens. This information, together with the knowledge of initial mesonic spectra, make it possible to extract the neutron skin thickness. Pionization studies may become a powerful method for studying nuclear surface because pionic charge measurements offer data that complement standard x-ray measurements.

DOI: 10.1103/PhysRevC.108.014313

I. INTRODUCTION

Hadronic atoms offer two main advantages for nuclear and low-energy particle physics:

(1) Studies of level shifts and widths allow us to test hadron-nucleon scattering amplitudes below the thresholds, since both particles are bound. In this way one could test the properties of exotic quasibound-states in two body systems.
(2) Atomic level shifts as well as studies of atomic decay modes of these systems are well-established methods for studying the structure of nuclear surfaces. The latter are particularly interesting in kaonic and antiprotonic atoms. In these cases nuclear absorption is very strong and orbiting particles are captured at extreme nuclear surfaces.

One point of interest is the possibility to study few nucleon correlations, another question is the existence of neutron haloes in neutron excess nuclei. This search has a long history. The existence of strong correlations at nuclear surface was brought forward by Wilkinson [1] a long time ago and was motivated by rapid captures of K^- mesons on two nucleons. In parallel neutron skins were studied with K-mesic atoms and found in heavy emulsion nuclei [2]. This line of research was found to be complicated by a strong resonant interaction in the $K^- p$ system and was not pursued further. Later, atomic studies were developed with intensive antiprotonic beams at CERN. Parallel to the x-ray measurements a different method was elaborated by a Munich-Warsaw collaboration [3]. The idea was to study nuclear residuals formed after $\overline{p}$ annihilation on (Z, N) nuclei. By radiochemical methods final $(Z-1, N)$ and $(Z, N-1)$ nuclei were detected, which made it possible to study the relative rates of $\overline{p}n$ and $\overline{p}p$ annihilations. As a result the number of neutrons relative to the number of protons in the capture region was extracted. Neutron haloes were detected in a large number of nuclides.

Complementary experiments, which we call "pionization," detected residual π mesons formed in antiproton annihilation. The pioneering experiment [4] measured the total charge Q of all mesons which managed to leave the nucleus. The charge distributions $P[Q]$ were determined and showed the usefulness of this method. Several experiments followed and we will discuss these in detail later. These early experiments were not analyzed in terms of nuclear structure. The necessary knowledge of $\overline{p}N$, πN, interactions and properties of antiprotonic atoms did not exist at that time. Now, such knowledge exists and we attempt to analyze these data. There is also another motivation for doing that. The pionization experiments are coming back with a much more ambitious purpose: namely to study neutron (or proton) haloes in radioactive nuclei. The first suggestion was to transport antiprotons in a portable trap from CERN to RIKEN and to form antiprotonic atoms of unstable nuclei there [5]. Now a modern version is being prepared at CERN as the PUMA experiment [6]. Our work presents a method for analyzing the expected experimental data. Potentialities and limitations are checked against the results of old experiments.

[*] slawomir.wycech@ncbj.gov.pl
[†] kristian.piscicchia@cref.it

When analyzing pionization and radiochemical measurements, an essential question is to learn from which atomic orbitals the nuclear capture occurs. In radiochemical measurements capture orbitals are determined by measurements of R_{A-1} (the fraction of final cold $A-1$ nuclei related to all capture events). Experiments yield $R_{A-1} \approx 0.1$, remarkably stable within a broad range of atomic numbers A. This indicates that captures leading to cold nuclei happen predominantly from "upper" atomic states, as also found in measurements of atomic x-ray cascades. The "lower" level is the lowest state reached by antiprotons which allows their energy to be determined by the line frequency and their width by the lineshape. Denoting the main and angular-momentum quantum numbers of this state by $(n_{\rm low}, L_{\rm low})$ the lower state is circular i.e., $(L_{\rm low} = n_{\rm low} - 1)$. The next circular state above it is called the "upper" state. Its energy is determined by the X-line energy and its width by intensity loss measurements. Atomic x-ray cascades are measured only in the low part of the process, but it is known that some antiprotons are captured from higher orbits. The value and stability of R_{A-1} allows also captures from higher n states provided that the angular momentum of these states equals the angular momentum of the upper level $l_{up} = l_{\rm low} + 1$. In the accessible states of the same angular momentum, but different main quantum numbers, the wave functions at nuclear distances differ only by normalization. For studies of nuclear surface all these states are equivalent. In this work we show that a similar capture rule applies to pionization measurements, but it is the lower state captures that prevail. Of course the distribution of capture states is the same in both experiments, it is the measurements that determine which states prevail in a given experiment.

To determine neutron haloes one also needs to know $R_{n/p}$ (the ratio of $\overline{p}n$ and $\overline{p}p$ annihilation rates). Low-energy antiprotonic experiments give $R_{n/p} = 0.48(10)$ in helium [7] and $R_{n/p} = 0.81(3)$ in deuterium [8]. The difference indicates the dependence of $R_{n/p}$ on nucleon and antiproton angular momenta, as well as the energy in the antiproton-nucleon center of mass system. We discuss this question in terms of the Paris $\overline{N}N$ potential model [9] and analyzes of atomic levels in the lightest nuclei [10]. It is shown that, at the nuclear surfaces, $R_{n/p}$ indicates a slow but systematic increase following the nuclear size. This trend is due mostly to increasing angular momenta of the antiprotonic capture levels. This enhances the effect of a fairly narrow (about 10 MeV) quasibound state in the P-wave $\overline{N}N$ system. The knowledge of the $R_{n/p}$ energy dependence, and a good model for the interaction involved, are important. Precise determination of neutron halo requires input of $R_{n/p}$ specific for each nucleus.

The present paper is organized as follows:

Section II introduces a model used to describe the formation of the emitted meson spectra $P[Q]$. Phenomenological parameters describing absorptions and charge exchanges of the final-state mesons are extracted from the existing data.

Section III presents a comparison of the phenomenological description with experimental data. The relation of the best-fit phenomenological parameters to the calculated values allows one to extract the dominant atomic antiproton capture orbits. Next, the thickness of the neutron skin is established for some nuclides.

Section IV summarizes advantages and weak points of the method.

Data and technical questions are presented in the Appendixes:

(A) Basic data describing mesonic spectra obtained from $\overline{p}n$ and $\overline{p}p$ annihilations at low energies are collected. Details of the phenomenological description are presented.

(B) Details of subthreshold extrapolations of $\overline{p}n$ and $\overline{p}p$ scattering amplitudes are given. Average absorptive scattering amplitudes in the atomic states of interest are calculated and the $R_{n/p}$ are given for all the pionization experiments.

(C) Final-state absorption and charge exchange of π mesons are discussed. Calculations of the phenomenological parameters in terms of pion-nucleus potential models and pion-nucleon charge-exchange cross sections are outlined. The effects of nucleon correlations are discussed.

II. THE METHOD FOR ANALYZING PIONIZATION EXPERIMENTS

The initial step is collection of necessary input data. We refer the reader to two reviews which present and discuss the reliability of some of the results used here. These consist of elementary [11] and nuclear [12] information. The first contains π meson multiplicities which are described by a matrix $M[k, m]$ giving emission probabilities of k $\pi^+, \pi-$ pairs and m neutral π^0 mesons. Such matrices are given in Appendix A for the basic single nucleon $\bar{p}p$ and $\bar{p}n$ annihilations. Nuclear data consist of $P[Q]$, i.e., the probabilities of total charge Q carried by mesons emitted in*nuclear* $\overline{p}$ captures. An additional essential quantity is the number of charged mesons emitted in a single antiproton capture event, which will be denoted by $\langle n^{\pm} \rangle$.

The analysis is done in three steps:

(1) In the first step we apply a simple phenomenological description of final-state interactions. The average chance for a charged π meson to leave the parent nucleus is introduced and denoted by T. The related small parameter $\omega = 1 - T$ is the probability that the meson is absorbed. Another small parameter λ describes the chance of a neutral π^0 meson to turn into a charge one. About five mesons are formed in a single capture. The initial charge distribution $P_{\rm ini}[Q]$ can be inferred from free antiproton-nucleon captures. The final distribution is expanded into a power series of λ and ω to account for interactions of the mesons. Next, the final distribution $P[Q]$ is compared with the experimental one and the best fit values of ω and λ are obtained. It turns out that, even in light nuclei, one has to use different parameters for different mesonic charges.

(2) In the second step the absorption and charge-exchange parameters are calculated with methods constrained by charge exchange and absorption antiproton-nucleus cross sections. These depend on the angular

TABLE I. The pion multiplicities $w_{\bar{p}p}$ for $\bar{p}p$ annihilation (in %).

n	2	3	4	5
$w_{\bar{p}p}$	0.38(0.03)	7.8(0.4)	17.5(3.0)	45.8(3.0)
n	6	7	8	
$w_{\bar{p}p}$	22.1(0.15)	6.1(1.0)	0.3(0.1)	

momentum of the capture states and are denoted by $\Omega(L)$ and $\Lambda(L)$. Comparison of best fit ω, λ with calculated $\Omega(L)$ and $\Lambda(L)$ allows one to determine two dominant L values of capture states. In this way one does not need to rely on x-ray cascade calculations. The latter are based on phenomenological estimates of the initial states of atomic capture. These are studied in solids or gasses [13,14], while PUMA measurements will be performed in vacuum.

(3) Based on the obtained capture states, the $R_{n/p}$ ratios are estimated and differences in the density mean square radii $R(n)_{ms} - R(p)_{ms}$ are calculated.

The phenomenological model assumes no correlations in the successive meson interactions. These are to be introduced in the next step. The phenomenological analysis is not in principle necessary, one could directly compare calculations to experimental data. Such a procedure is, however, complicated by the uncertainties affecting both the old data sets and the details of the final-state interaction description. The phenomenological approach rests on a more solid ground and allows some degree of control over both these uncertainties.

A. Phenomenological analysis

In this section the first step undertaken to understand pionization is presented. First we collect data on the spectrum of meson formation process and then we describe the emission and final-state interactions of the pions.

Let us begin with the primary data of antiproton-nucleon annihilation into π mesons. We describe the nuclear data by means of a parametrization in terms of average single meson loss and charge-exchange probabilities. The $\bar{p}p$ annihilation starts with the process

$$\bar{p}p \to \pi_1 \ldots \pi_n, \tag{1}$$

and the number of mesons extends from multiplicity $n = 2$ until $n = 8$ [11], as summarized in Table I.

An initial step of annihilation may involve π mesons correlated into vector mesons. The effect of such correlations on the nuclear capture studies has been discussed in Ref. [15] and leads to some extension of the capture region, but has a rather limited effect on the scenario of the mesonic final interactions. We postpone the study of correlation effects to future analyses of more refined experimental data sets.

In the free space, the total charge carried by mesons in $\bar{p}p$ capture is $Q = 0$. We normalize the rate of this process in nucleus to be 1 and refer other rates relative to this:

$$P_{\rm ini}[Q = 0] = 1. \tag{2}$$

With this normalization the rate of initial $\bar{p}n$ annihilations is *defined* as

$$P_{\rm ini}[Q = -1] = \frac{N}{Z} R_{n/p} f^h, \tag{3}$$

where N (Z) is the number of neutrons (protons) in the nucleus. The *halo factor* f^h was introduced by Bugg *et al.* [16] to represent an additional excess of neutrons over protons in the capture region. Let us stress that f^h has no universal value because it depends on the initial atomic capture state as well as on the experimental method chosen to detect the final products: residual, mesons, or x rays.

Final-state mesonic interactions change the distribution of the charge spectrum to the experimentally measured $P[Q]$. The practically irreversible processes are the "true meson absorptions" on nucleon pairs:

$$\pi^+ NN \to N'N', \quad \pi^- NN \to N'N', \tag{4}$$

but also other reactions:

$$\pi^+ n \to \pi^0 p, \quad \pi^- p \to \pi^0 n, \tag{5}$$

contribute to the reduction of the number of emitted charged mesons. Two parameters ω^+ (for π^+) and ω^- (for π^-) are introduced to describe cumulative loss due to both absorption and charge exchange, they slightly differ even for $Z = N$ nuclei. Inverse reactions to those described by Eq. (5) are induced by neutral mesons, produced in the initial antiproton annihilation, and increase the total number of emitted charged mesons

$$\pi^0 p \to \pi^+ n, \quad \pi^0 n \to \pi^- p. \tag{6}$$

The parameters λ^+ and λ^- describe corresponding average π^0 charge exchanges.

By isospin symmetry the direct (5) and the inverse (6) reactions offer the same transition amplitudes but do not balance each other in the nuclear systems studied here, hence, they have then to be considered separately. The interplay of the two processes is one of the crucial and difficult problems of the pionization experiments. To deal with this issue one has to disclose the charge spectra hidden inside the multiplicity distributions. This is accomplished by the introduction of spectral matrices:

(1) $MP[k]$ and $MN[k]$ give the probability to emit k (π^+, π^-) pairs in $p\bar{p}$ annihilations and k (π^+, π^-) plus a π^- in $n\bar{p}$, respectively. Both are obtained from bubble-chamber measurements [17] and magnetic spectrometer measurements [18].

(2) $MP[k, m]$ and $MN[k, m]$ give related probabilities for the production of m neutral pions. The latter are harder to obtain and information from an in-flight experiment [19] is to be used.

All matrices and related uncertainties are discussed in Appendix A. Normalization is consistent with the initial normalization (2)

$$\sum_k MP[k] = 1, \quad \sum_m MP[k, m] = 1,$$
$$\sum_{k,m} MP[k] MP[k, m](2k) = \langle n^{\pm} \rangle. \tag{7}$$

In nuclear studies only charged mesons are detected and it is essential to consider also the average numbers of produced charged mesons $\langle n^{\pm}\rangle$. For $\bar{p}p$ annihilation $\langle n^{\pm}\rangle = 3.18(10)$ and for $\bar{p}n$ annihilation $\langle n^{\pm}\rangle = 3.28$, obtained from experiments [18] and [17]. In cases of nuclear captures the corresponding $\langle n^{\pm}\rangle$ become smaller reflecting true annihilations of charged mesons on correlated nucleon pairs and losses due to charge exchanges into neutral mesons. Comparison of the nuclear $\langle n^{\pm}\rangle$ with the elementary ones becomes the main indicator of annihilation regions. The pionization in nuclei can be parametrized in terms of total charge spectra, which give probability of total charge Q carried out by the mesons. Experiments offer $P[Q]$, which in principle yield rich information on the nuclear structure. We attempt to extract this information and assess the related reliability.

1. Expansion of P[Q] in the number of mesic collisions

Nuclear pionization data provide up to eight experimental quantities per nuclear target; these represent probabilities of the total emitted charge $P[Q]$, plus the information on the total number of charge mesons $\langle n^{\pm}\rangle$ emitted in a single antiproton annihilation event. The best studied targets are lead and carbon, but the most precise measurement was performed using nitrogen. Available data are summarized in the next sections.

Consider antiprotonic annihilation on a proton bound to a nucleus. The initial $P[Q]$ distribution has only $Q = 0$ component given in Eq. (2). This probability is reduced from its primary value by the chance that some mesons do not leave the nucleus. Let us denote the meson transmission probabilities by T^+ and T^- for the π^+ and π^-, respectively. The chance to see final charge $Q = 0$ is

$$\Delta P[0] = \sum_{k,m} MP[k]MP[k,m](T^+)^k(T^-)^k(T^0)^m, \quad (8)$$

where we introduce the probability T^0 that a neutral π^0 meson does not change sign. The primordial charge mesons might be lost. Two parameters describing the rate of losses ω^- and ω^+ are related to the transmission probabilities by

$$T^+ = 1 - \omega^+ \text{ and } T^- = 1 - \omega^-. \quad (9)$$

Reactions (4) and(5) contribute to the absorption of charged mesons. Now if one π^- disappears in the final state one obtains a contribution to the $P[Q = +1]$ channel equal to

$$\Delta P[1] = \sum_{k\geqslant 1,m} MP[k]MP[k,m](T^+)^k(T^-)^{k-1}(T^0)^m\omega^-, \quad (10)$$

and similarly if two π^- are lost one has

$$\Delta P[2] = \& \sum_{k\geqslant 2,m} MP[k]MP[k,m](T^+)^k(T^-)^{k-2}(T^0)^m(\omega^-)^2. \quad (11)$$

Continuation of this procedure includes the loss of three mesons. In all formulas ΔP indicates the final summation of all possible outcomes.

In a similar way one calculates losses of positively charged mesons. If a π^+ disappears in the final-state one obtains a contribution to the $P[-1]$ channel equal to

$$\Delta P[-1] = \sum_{k\geqslant 1,m} MP[k]MP[k,m](T^+)^{k-1}(T^-)^k(T^0)^m\omega^+, \quad (12)$$

and similarly for the loss of two or three π^- mesons.

Let us turn to another process which begins with the primary $\bar{p}n$ capture. The spectral probabilities are normalized by conditions

$$\sum_k MN[k] = 1, \quad \sum_m MN[k,m] = 1,$$
$$\sum_{k,m} MN[k]MN[k,m](2k+1) = \langle n^{\pm}\rangle. \quad (13)$$

In the former proton reaction, we assumed the primordial probability $P_{\text{ini}}(Q = 0) = 1$ [Eq. (2)]. Now, for an easy comparison, we include the neutron excess and $R_{n/p}$ into the definition of the primordial channel distribution [Eq. (3)] and it becomes evident that the essential result of this analysis is a product of $R_{n/p}f^h$. In the quantum description developed later, or with sequential studies of many nuclei one might have independent constrains on $R_{n/p}$ and f^h. At this stage of the pionization experiments one has to introduce $R_{n/p}$ from other experiments, keeping in mind that it is dependent on the atomic and nuclear state of capture. The probability $\Delta P[-1]$ to observe final $Q = -1$ due to capture on neutrons becomes

$$\Delta P[-1] = R_{n/p}\frac{N}{Z}f^h\sum_{k,m} MN[k]MN[k,m] \times (T^+T^-)^k(T^-)^1(T^0)^m. \quad (14)$$

Now if one of π^- is absorbed in the final-state one obtains a contribution to the $P[Q = 0]$ channel equal to

$$\Delta P[0] = R_{n/p}\frac{N}{Z} \times f^h\sum_{k,m} MN[k]MN[k,m](T^+T^-)^k(T^0)^m\omega^-. \quad (15)$$

This procedure is continued up to the third order in the absorption events.

An initial π^0 meson may be changed to a charged one which gives an additional contribution to $P[Q]$. The rate of π^0 mesons turning into π^+ via reaction (6) will be described by the parameter λ^+. With an initial $p\bar{p}$ annihilation beginning with $Q = 0$ this process enhances the rate in $Q = 1$ channel by

$$\Delta P[1] = \sum_{k,m\geqslant 1} MP[k]MP[k,m] \times (T^-)^k(T^+)^{k+1}(T^0)^{m-1}\lambda^+. \quad (16)$$

The related reaction $\pi^0 n \to \pi^- p$ is described by another parameter λ^-.

At this stage we have to introduce a kind of self-consistency condition. Reactions (4) and (5) generate loss of charged mesons and reactions (6) generate gains of such

mesons from neutral mesons. Competition between these processes forces us to introduce a third parameter ω^0 describing a net loss of a single π^0 related to its transmission probability

$$T^0 = 1 - \omega^0. \tag{17}$$

The phenomenological values of ω^0 turn out close but different from ω^+ or ω^-.

The procedure is extended up to third order in the free parameters and thus contains terms up to ω^3, λ^3, $\omega^2\lambda$, $\omega\lambda^2$ which cover all experimental values of Q. The values of $M[k]$, $M[k,m]$ are listed in Appendix A. Calculated rates $P[Q]$, due to both $p\bar{p}$ and $n\bar{p}$ captures, are normalized, for each channel, to the total probability. They are then compared with the experimental probabilities and the parameters ω^+, λ^+, ω^-, λ^-, ω^0, and $R_{n/p}f^h$ are obtained by a best-fit procedure.

In the next section the best-fit parameters are presented. The theoretical analysis is given in Appendix C where the way to calculate λ and ω is presented. The calculated values are denoted by capital Λ and Ω to distinguish them from the best-fit values.

III. ANALYSIS OF EXPERIMENTAL DATA

The pionization experiments were performed with two detection techniques: hydrogen (and freon) chamber measurements performed on C, Ti, Ta, Pb targets and magnetic spectrometer measurement done in nitrogen.

A. Old bubble-chamber measurements

These pionization measurements were performed in carbon [4,16,20], titanium, tantalum and lead [16]. The purpose of this section is the extraction of neutron haloes in a quantitative way. Unfortunately, the old measurements offered only 10^3–10^4 events per target, which is two orders of magnitude less than the nitrogen experiment. In addition, the $P[Q]$ spectrum is contaminated by events of capture on some hydrogen present in the chambers. The analyzed nuclei have different structure, which allows one to test three circumstances: light nuclei, neutron excess nuclei, and deformed nuclei. The leading calculations presented in Sec. II A allow us to analyze the available experimental information. Possible fine structures, due to proton-neutron and α-particle correlations are estimated in Appendixes C 3 and C 4. First we outline the procedure which is used to extract the capture state and neutron haloes.

1. Extraction of neutron haloes

The first step is to establish the capture states. The best-fit values of absorption and charge-exchange parameters are obtained from the measured Q spectra and total numbers of emitted mesons. It is argued in Appendix C 5 that the best understood parameters are sums $\lambda = \lambda^- + \lambda^+$ and as a consequence also $\omega = \omega^+ + \omega^-$. These combinations reduce errors due to uncertain multiplicities of π^0 mesons and proton-neutron correlation effects. Thus, we calculate the charge-exchange rates $\Lambda(L)$ for several orbits characterized by L and compare these with the best-fit value. Next we find angular momentum L_d which allows us to straddle the best-fit experimental value,

$$\Lambda(L_d + 1) < \lambda < \Lambda(L_d). \tag{18}$$

This relation is used to find probabilities of capture from two dominant towers of capture orbits $P(L_d)$ and $P(L_d + 1)$ fixed by normalization $P(L_d) + P(L_d + 1) = 1$. Similar relations for the sum of loss parameters

$$\Omega(L_d + 1) < \omega < \Omega(L_d) \tag{19}$$

are expected to hold with the same L_d and to allow better verification of the selected orbits and check inconsistencies. The probability values obtained from Eqs. (18) and (19) are averaged.

In principle, the knowledge of capture states and halo factors f^h allows nuclear theorists to check nuclear surface structure models. However, in order to facilitate this procedure, experimental findings have usually been presented in terms of mean square radii of nuclear density distributions. This procedure is followed here. Halo factors f^h are obtained from the best fit values of $R_{n/p}f^h$ and $R_{n/p}$ is taken from other experiments. The latter are checked against atomic x-ray experiments, nuclear absorption experiments, and extrapolated from scattering cross sections in terms of a model. Appendix B presents a way to achieve this in terms of the Paris potential model [9].

Next, one can use f^h to compare proton and neutron density distributions. The way usually adopted is to use a test neutron density containing one free parameter, for example half density radius, surface thickness or mean square radius. Next, this parameter is fixed by the experimental f^h and the outcome is presented as a difference

$$\Delta R = R_{ms}(n) - R_{ms}(p), \tag{20}$$

where R_{ms} are the mean square radii of proton and neutron density distributions. Without a specific nuclear model such procedure is not unique. Here, we follow the findings of radiochemical experiments [21], and look for haloes as changes of surface parameters a in the two parameter Fermi density profile

$$\rho(r, c, a) = \frac{\rho_0}{1 + \exp\left[(r - c)/a\right]}. \tag{21}$$

The surface thickness of charge distribution is well known from electromagnetic studies [22]. To get proton densities one has to unfold the electric form factor of the proton. It is easy for a given moment of charge distribution and it is customary to concentrate on R_{ms}—the mean square radius—which fulfils the relation

$$R^2_{ms}(p) = R^2_{ms}(c) - r^2_{ms}(p), \tag{22}$$

where $r_{ms}(p) = 0.875$ fm is the mean square charge radius of the proton density. This radius should be compared with the neutron density radius $R_{ms}(n)$. This presents a technical problem, the resolution of the proton density from the experimental charge density is not easy. The difficulty may be removed when one notices that the annihilation radius in the nucleon antinucleon system is roughly equal to the charge radius of the proton. In addition the optical potential describing antiproton absorption in nuclei is obtained by folding

the "bare" nuclear density over the annihilation range [23]. In particular, an optical potential adapted to fit x-ray data finds a folding range of 0.79 fm [24]. As the range of absorptive interaction is comparable to the proton charge radius we use charge distribution to describe capture on protons and compare these with the folded distribution for neutrons. Formula (22) indicates that the difference $R_{ms}(n) - R_{ms}(p)$ is essentially the same for folded and "bare" densities. So the densities used in equation (23) are the folded densities which are equal to charge densities in the proton case. We also assume the annihilation radii in $\overline{p}n$ and $\overline{p}p$ pairs to be the same, an assumption well fulfilled in the Paris potential models. A bit weaker is our next assumption, namely that the half density radii for protons and neutrons are the same $c_p = c_n$. It is based on the radiochemical experiments which find that neutron haloes description in terms of $c_n - c_p$ is rejected by the data [21]. Of course, this assumption is not to be used when data are compared with more involved nuclear models. However, on a phenomenological level there is only one parameter that may be fixed by one experimental number f^h.

Now, the calculated halo factor $f^h(L, a)$ is given by ratio of two overlap integrals yielding the capture rates on a proton and capture rates on a neutron:

$$\Theta_i(L, c_i, a_i) = \int d\mathbf{r}|\psi(r)_L|^2 \rho(r, c_i, a_i), \tag{23}$$

where i stands for neutron or proton and the nuclear densities are normalized to unity. ψ_L is the atomic wave function of an antiproton. For a given angular momentum L we have

$$f^h(L, a_n) = \frac{\Theta(L, c_c, a_n)}{\Theta(L, c_c, a_c)}. \tag{24}$$

With the method presented here one extracts probabilities $P(L)$ for the two dominant values of L. Hence, the thickness of neutron surface a_n is obtained from a more involved relation to the experimental halo f^h

$$f^h(L_d, a_n)P(L_d) + f^h(L_d + 1, a_n)P(L_d + 1) = f^h, \tag{25}$$

where L_d is determined by conditions (18) and (19). The a_n allows us to calculate the R_{ms} of the folded neutron distribution. With the help of relation (22) applied to folded neutron distributions and to charge distributions, one calculates ΔR of Eq. (20). The effects of folding range and proton charge radius cancel to a negligible contribution.

2. Carbon, a question of hydrogen contamination

The proton and neutron radii in carbon are apparently very similar and this nucleus was used as a testing ground to obtain $R_{n/p}$. We can take advantage of two independent measurements performed in a hydrogen chamber by Bugg *et al.* [16] and in a freon chamber by Wade and Lind [20]. The parameters obtained from the fit of the freon data (which are reported in the second column of Table II) are summarized in Table III; they indicate capture happening from a mixture of $L = 2$ and $L = 3$ states. As described in Sec. III A 1, when calculating the relative proportion of these states it is prudent to use sums of two charges for λ and ω. Charge exchange favors upper L and absorption favors lower L, and the average result is $P(L = 3) = 0.45, P(L = 2) = 0.55$. It compares well with the low end of the x-ray cascade measurements. Reference [25] finds approximately equal rates of capture from the $4f$ and $3d$ states. Assuming the same proton and neutron density distributions our analysis suggests $R_{n/p} = 0.75(0.01)$, the Paris potential (Table XVIII) yields $R_{n/p} = 0.698$ closer to the early results of Bugg and Wada-Lind, $R_{n/p} = 0.63(0.03)$.

TABLE II. Experimental and fitted charge multiplicities $P[Q]$ in carbon. The second column refers to freon [20] and the fourth column to hydrogen-chamber [16] experiments. The numbers are taken from review [18], which includes hydrogen background subtraction and provides error bars.

Q	C [20]	Fit	C [16]	Fit
+3	0.09(0.1)	0.09	0.2 (0.1)	0.2
+2	1.80(0.2)	1.36	2.1(0.2)	2.1
+1	12.5(0.4)	13.02	17.5(0.5)	15.2
0	43.0(0.8)	44.49	38.3(0.8)	41.7
−1	34.5(0.7)	33.90	33.7(0.7)	31.3
−2	6.5(0.5)	6.84	7.8(0.3)	8.6
−3	1.0(0.1)	0.28	0.6(0.1)	0.8
$\langle n^{\pm}\rangle$	2.72(0.03)	2.70	2.79(0.04)	2.79
χ^2		13.1		61 .1
$R_{n/p}f^h$		0.75(0.01)		0.64(0.03)

The two experimental results obtained in carbon differ by many standard deviations in the dominant proton absorption $Q = 0$ channels. The difference indicates problems with hydrogen contamination. In the basic hydrogen chamber experiment contamination is estimated and subtracted from the data but no error is provided. This uncertainty is reflected in all hydrogen chamber experiments, which are discussed below. With the method developed here we find vastly inferior fit to the hydrogen chamber data.

3. Titanium

Titanium is a medium sized nucleus which develops some neutron excess. In this section the capture orbit and the neutron density radius are extracted in $^{48}_{22}$Ti. Experimental results [16] are summarized in Table IV. The correction due to hy-

TABLE III. C atom. Pion absorption and charge-exchange parameters. Calculated and the best fits to the freon chamber experiment [20].

	$\Lambda(3)$	Fit λ	$\Lambda(2)$
λ^+	0.14	0.19(.02)	0.194
λ^-	0.14	0.12(.02)	0.194
$\lambda^- + \lambda^+$	0. 280	0.31(.03)	0.388
	$\Omega(3)$	Fit ω	$\Omega(2)$
ω^0		0.12(0.03)	
ω^+	0.087	0.12(0.01)	0.140
ω^-	0.087	0.14 (0.01)	0.140
$\omega^+ + \omega^-$	0.174	0.26 (0.02)	0.280

TABLE IV. Experimental charge multiplicities $P[Q]$ in ^{48}Ti from Ref. [16]. The second column gives number of events. $P[Q]$ values are summarized in the third column, accounting for the subtraction of hydrogen contamination and experimental errors, according to the review [12]. The fourth column shows the result of our fit.

Q	Nb. events	$P[Q]$ %	Fit
3	6	0.3(0.1)	0.33
+2	54	2.5 (0.3)	2.68
+1	391	17.9(0.8)	14.62
0	927	32.6(1)	36.42
−1	784	36.0(1)	34.62
−2	209	9.6(0.6)	10.50
−3	23	1.1(0.2)	0.58
−4	2	0.1(0.1)	0.00
$\langle n^{\pm}\rangle$		2.58(0.07)	2.54
χ^2			65.0
$R_{n/p}f^h$			1.23 (0.10)

drogen contamination (which amounts to 9.1%), reduces the multiplicity of the $Q = 0$ channel. The total λ and ω values obtained from the fit are reported in Table V. The fit is bad, in particular in the $Q = 0$ channel and this might be related to uncertain hydrogen background. The same effect is apparently reflected in the anomalously large value of the fitted λ. The latter violates limits (18). To go further we set $P(L = 4) = 1$ and continue with the limits (19). It generates average $P(4) = 0.82$ and $P(5) = 0.18$ which is predominantly capture from lower states. Measurements of x-ray cascade in Ti were attempted but the lower $5g$ state has not been reached [26]. In the nearby Ca the $4f$ is found to be the lower state but the dominant capture state detected in the x-ray cascade is $L = 4$ [27]. Hence, one expects the capture states in Ti to be a mixture of $L = 4$ and $L = 5$ as a consequence of a bigger nuclear charge.

To extract the neutron radius we use the capture probabilities extracted above, the value $R_{n/p}f^h = 1.23(0.10)$ which is obtained from the fit and $R_{n/p} = 0.774$ from Table XVIII. These yield the halo factor $f^h = 1.59(0.13)$, which corresponds to a surface density difference $a_n(n) - a_n(p) = 0.082(0.02)$ fm and ultimately to a halo thickness $R_{ms}(n) - R_{ms}(p) = 0.17(0.04)$ fm. The error is determined

TABLE V. Ti atom. Pion absorption and charge-exchange parameters. Calculated and the best fits to the hydrogen chamber experiment.

	$\Lambda(5)$	Fit λ	$\Lambda(4)$
λ^+	0.197	0.34(.02)	0.262
λ^-	0.166	0.16(0.01)	0.193
$\lambda^- + \lambda^+$	0.363	0.50(0.02)	0.455
	$\Omega(5)$	ω	$\Omega(4)$
ω^0		0.14(.02)	
ω^+	0.140	0.18(.02)	0.180
ω^-	0.162	0.19(0.02)	0.228
$\omega^+ + \omega^-$	0.302	0.37(0.02)	0. 408

TABLE VI. The experimental charge multiplicities $P[Q]$ in ^{181}Ta are summarized in the second column, the result of the best fit is reported in the third column.

Q	$P[Q]$	Fit
3	0.2(0.1)	0.37
2	3.4(0.4)	2.84
1	18.1(0.8)	12.42
0	27.3(1)	32.37
−1	38.8(1)	37.16
−2	10.7(0.7)	14.17
−3	1.5(0.3)	0.63
$\langle n^{\pm}\rangle$	2.47(0.08)	2.44
χ^2		83.8
$R_{n/p}f^h$		2.00(0.23)

by the uncertainty on the $R_{n/p}f^h$ value given by the fit. Another source of uncertainty is the value of $R_{n/p}$ obtained from the Paris potential. Had we followed $R_{n/p} = 1$ used in analyses of x-ray experiments with heavy nuclei [23,28] $R_{ms}(n) - R_{ms}(p) = 0.075(0.03)$ fm would follow. This indicates importance of a well-tested $\overline{N}$-N interaction model. The case of titanium is poorly understood.

4. Tantalum

This section analyzes experiment with $^{181}_{73}$Ta. Experimental results and related analysis resemble the case of titanium although these nuclei strongly differ. The $P[Q]$ data from hydrogen chamber [16] supplied with error estimate from review [12] are shown in Table VI, together with our fit. The channels $Q = 0, 1$ are not well described, possibly due to uncertain hydrogen contamination, but another possibility is also discussed below. The parameters λ and ω obtained from the fit are reported in Table VII and compared with the calculated values.

Calculations of Λ and Ω were performed using standard charge distribution [22] that assumes spherical symmetry. The comparison of the calculations with the best fit, for the summed λ and ω values, yields capture probabilities $P(L = 7) = 0.38$, $P(L = 8) = 0.62$. The individual assessments, based separately on λ and on ω, differ sizably, possibly because the nucleus is deformed while the calculations of

TABLE VII. Pion absorption and charge exchange parameters obtained from calculation and fit to the ^{181}Ta atom data.

	$\Lambda(8)$	Fit λ	$\Lambda(7)$
λ^+	0.240	0.42 (0.03)	0.288
λ^-	0.277	0.15 (0.02)	0.308
$\lambda^- + \lambda^+$	0.517	0. 57 (0.03)	0.596
	$\Omega(8)$	ω	$\Omega(7)$
ω^0		0.275	
ω^+	0.159	0.18	0.192
ω^-	0.192	0.18	0.252
$\omega^+ + \omega^-$	0.351	0.36	0. 444

final-state mesonic interactions were performed assuming Ta to be spherical. With the Paris potential prediction $R_{n/p} = 0.889$ (Table XVIII) one has $f^h = 2.28(0.25)$ fm. In contrast to the case of Ti this prediction of $R_{n/p}$ has strong support from x-ray measurements. The halo parameter is large and corresponds to excess of neutron surface density $a_n - a_p = 0.097(0.012)$fm, calculated with charge-density parameters $c_c = 5.156$, $a_c = 0.5342$ fm [22]. It corresponds to $R_{ms}(n) - R_{ms}(p) = 0.17(0.03)$ fm.

Cascade measurements in Ta ($Z = 73$) are not available, the "nearest" x-ray experiment was performed in ^{172}Yb ($Z = 70$) [14] accompanied by the radiochemical measurement in ^{176}Yb [21]. The x-ray cascade reaches $n = 8$, $L = 7$ because the lowest circular state and the bulk (70%) of captures happens in the $L = 8$ circular state [14]. It is consistent with our results in Ta. However, all these nuclei are deformed, atomic levels are mixed due to $E2$ excitations of nuclear rotations and the cascade processes might differ. A problem, and perhaps also an advantage arises for the pionization studies. Let us present only one aspect of this possibility. Halo factors have been measured in three deformed nuclei: ^{160}Ga, ^{176}Yb [21], and ^{181}Ta [16]. The corresponding values of $R_{n/p}f^h$ are 3.655(1.12), 5.04(0.38), and 2.28(0.22) ($R_{n/p} = 0.63$ was used in Ref. [21], hence we compare $R_{n/p}f^h$). One finds a large difference in the values extracted from the radiochemistry (Ga, Yb) and from the pionization (Ta). Possibly this is due to sizable differences in the deformations. Thus in the first two nuclei $\beta_2 = 0.33$ [22] and the value *calculated* for ^{181}Ta is $\beta_2 = 0.25$ [29] and that extracted from muonic atoms is $\beta_2 = 0.27$ [22]. The halo factor is apparently strongly dependent on deformation. The bad fit given in Table VI and calculation performed on a spherical model for Ta nucleus prevent stronger statements. However, more precise experiments and better analyses may determine if is it the central core or the halo which is deformed.

5. Lead

Lead is the most investigated nuclear target used for experimental determinations of neutron haloes. The pionization data shown in Table VIII allow comparison with other experiments. The comparison of calculation, with the parameter values obtained from the fit, is shown in Table IX. The last bin in the tail of the $P[Q]$ distribution, corresponding to $Q = -3$, is not considered in the fit since it considerably worsens the χ^2. The extracted capture probabilities become $P(L = 8) = 0.71$, $P(L = 9) = 0.39$ and are consistent with the intensities of the lowest x-ray transitions indicating $n = 9$, $L = 8$ to be the lower state [28]. In the lower part of cascade this measurement indicates about 2/3 of captures to occur from the lower state and 1/3 of captures to occur from the upper state.

From the outcome of the fit and $R_{n/p} = 0.92$, obtained from Paris potential for captures in the $L = 9$ state, we obtain $a_n - a_p = 0.13(.035)$ fm and $R_{ms}(n) - R_{ms}(p) = 0.20(0.03)$ fm. A similar result was obtained in the x-ray measurements [28] $R_{ms}(n) - R_{ms}(p) = 0.16 \pm (0.02) \pm (0.04)$ fm under the assumption $R_{n/p} = 1$, which follows from global x-ray data analyzed with an optical potential [23]. This indicates that an improved control on the uncertainty of $R_{n/p}$ is important, but not essential in the case of Lead and possibly also in other heavy nuclei.

TABLE VIII. The experimental charge multiplicities $P[Q]$ in Pb are summarized in the second column. Data correspond to Ref. [16], the subtraction of 11% hydrogen contamination and experimental errors follow review [12]. The result of the fit is summarized in the third column.

Q	$P(Q)$ %	Fit
+3	0.1(0.1)	0.33
+2	2.6 (0.4)	2.88
+1	15.1(0.9)	13.11
0	30.6(1.7)	33.73
−1	37.7(1.2)	36.90
−2	12.3(0.8)	12.52
−3	1.7(0.3)	0.50
$\langle n^{\pm}\rangle$	2.44(0.04)	2.44
χ^2		10.6
$R_{n/p}f^h$		2.10(0.23)

6. Average final-state pion absorption probabilities

Table X presents the average final-state pion absorption probabilities obtained in the hydrogen chamber experiment of Bugg*et al.* These values were obtained by comparing the measured $\langle n^{\pm}\rangle$, with the average numbers of charged mesons produced in the elementary $\bar{p}p$ and $\bar{p}d$ reactions. Table X also shows the probabilities obtained in the present analysis, from the simultaneous fit of the $\langle n^{\pm}\rangle$ and $P(Q)$ distributions. These present the best-fit numbers of ω^+ and ω^-, weighted by the primordial numbers of π^+ and π^- mesons.

B. Nitrogen experiment

The measurement performed in nitrogen [18] has several advantages: it offers the highest statistics obtained so far, is free from the hydrogen contamination, and presents experimental errors. On the other hand, the nitrogen nucleus is specific in its structure. The atomic cascade is also specific as the experiment is performed in a gaseous target. It deserves special attention and detailed theoretical calculations.

TABLE IX. Pb atom. Pion absorption and charge exchange parameters. Calculated and the best fits to the hydrogen chamber experiment.

	$\Lambda(9)$	Fit λ	$\Lambda(8)$
λ^+	0.263	0.42(.03)	0.309
λ^-	0.234	0.13(0. 03)	0.248
$\lambda^- + \lambda^+$	0.497	0.55 (0.03)	0.55
	$\Omega(9)$	ω	$\Omega(8)$
ω^0		0.230	
ω^+	0.131	0.20(0.01)	0.150
ω^-	0.231	0.200(0.01)	0.287
$\omega^+ + \omega^-$	0.362	0.40(0.01)	0.437

TABLE X. Comparison of average meson absorption in the final state, obtained in Ref. [16] and results of this work.

	C	Ti	Ta	Pb
Bugg *et al.*	0.110(0.01)	0.174 (0.01)	0.211(0.012)	0.221(0.014)
This work	0.125	0.180	0.180	0.20

Table XI summarizes the fit results for the charge probability distribution. The best-fit parameters are shown in Table XII.

The best fit to charge-exchange parameters λ indicates the initial capture spread over three L values. However, the $L = 1$ component which may be generated by Stark mixing in upper levels of x-ray cascade is minute and is not supported by ω. According to the same procedure applied in the Ti case we obtain $P(2) = 0.74$, $P(3) = 0.26$. Calculations of atomic cascade in a nitrogen atom are not available but the lowest transitions are known from Poth's measurement [30]. It was found that captures from circular $4f$ state and from lower circular $3d$ state are roughly in proportion 55 : 45. The pionization experiment favors lower $L = 2$ states that is as in other atoms, but nitrogen might differ for another reason. The pionization experiment was performed in gas while the x-ray experiment was performed in liquid nitrogen. The initial state of atomic capture and the course of x-ray cascade differ in those two experiments.

Having established the capture orbits one may calculate the difference of proton and neutron density radii. With the best fit $R_{n/p}f^h = 0.61(0.04)$ and $R_{n/p} = 0.72$, obtained with the Paris potential, one obtains halo factor $f^h = 0.85(0.05)$ that is a weak preference for an enhanced proton tail. The proton-neutron R_{ms} difference of 0.01(0.005) fm follows. The experimental separation energies for valence nucleons in the N nucleus are $S(n) = 10.5$, $S(p) = 7.5$ MeV and $S(2n) = 35.1$, $S(2p) = 25.1$ MeV, which give some support to the obtained result.

The error of R_{ms} is mainly due to the uncertainty of f^h, but there are other contributions. The calculation in terms of noncorrelated subsequent collisions fails to describe the $Q = \pm 3$ tails of the experimental $P[Q]$ charge distribution. These could be generated by the peculiar carbon structure of the nitrogen nucleus core, characterized by strong three α-type correlations. Such a structure may enhance the probability of the $Q = \pm 3$ channels in the final mesonic charge spectrum. A simple model for such mechanism is discussed in Sec. C 4, it is based on double pionic charge exchange which is frequent in α particles. We repeated the fit to the $P[Q]$ spectrum by adding a small correction estimated in Sec. C 4. The result is presented in the fourth column of Table XIII and compared with the experimental distribution and the result of the previous fit. Inclusion of double charge exchange considerably improves the fit results but does not change the $R_{n/p}f^h$. An open question is the possibility to establish the presence of alpha particles on nuclear surface. The crude model presented here indicates such a possibility. The basic condition is a reliable model for the π-α double charge-exchange cross section in the 300–400 MeV range of the pion kinetic energies.

TABLE XI. Experimental [18] and fitted charge multiplicities $P[Q]$ in nitrogen.

Q	Expt	Fit
+3	1.2(0.2)	0.21
+2	3.9(0.4)	2.02
+1	14.2(0.8)	14.74
0	39.5(1.0)	41.54
−1	31.1(0.8)	31.59
−2	8.0(0.5)	8.76
−3	2.1(0.3)	1.01
$\langle n^{\pm}\rangle$	2.89(0.08)	2. 89
χ^2		67.8
$R_{n/p}f^h$		0.61(0.04)

TABLE XII. The table shows calculated and best-fit results for the pion absorption and charge-exchange parameters in the case of a nitrogen target.

	Λ(3)	Fit λ	Λ(2)
λ^+	0.179	0.25(.02)	0.247
λ^-	0.164	0.24(0.02)	0.212
$\lambda^- + \lambda^+$	0.353	0.49 (0.03)	0.459
	Ω(3)	ω	Ω(2)
ω^0		0.196	
ω^+	0.088	0.125	0.116
ω^-	0.104	0.145	0.180
$\omega^+ + \omega^-$	0.192	0.270	0.296

IV. CONCLUSIONS AND OUTLOOK

Investigating old experimental data we show that pionization measurements may become a profitable source of information on nuclear surfaces in stable and in unstable nuclei.

1. Advantages

The advantage of this method is that it offers many independent measurable quantities: seven final mesonic charge

TABLE XIII. Experimental [18] and fitted charge multiplicities $P[Q]$ in nitrogen. The last column includes double charge exchange calculated in a 3α model of residual nucleus.

Q	Expt	Fit	Fit + 2-chex
3	1.2(0.2)	0.21	0.63
+2	3.9(0.4)	2.02	3.04
+1	14.2(0.8)	14.74	14.54
0	39.5(1.0)	41.54	41.00
−1	31.1(0.8)	31.54	30.84
−2	8.0(0.5)	8.8	8.44
−3	2.1(0.3)	1.01	1.46
$\langle n^{\pm}\rangle$	2.89(0.08)	2.89	2.89
$R_{n/p}f^h$		0.61(0.04)	0.61(0.04)
χ^2		67	19

channels $P[Q]$ and total number of emitted charge mesons $\langle n^{\pm}\rangle$. These data allow us to extract two important outcomes of the analysis:

(1) the atomic levels from which the nuclear capture of antiprotons occurs;
(2) the neutron excess in the capture region is obtained, provided $R_{n/p}$—the ratio of $(\overline{p}n)$ and $(\overline{p}p)$ annihilation rates—is known from other experiments.

In the next step one can calculate the neutron haloes in nuclei and present these in terms of radius mean square differences $R_n - R_p$. The knowledge of nuclear capture orbits is significant as the x-ray cascade calculations are not very precise. Cascades are checked in solid or gas targets. Similar studies in vacuum, to be met in the PUMA experiment, have no such advantage.

To obtain satisfactory precision of these results one needs to control charge-exchange rates $\pi^+ \to \pi^0$ and $\pi^- \to \pi^0$ in nuclei. Precise calculations of these are difficult due to the effects of Pauli principle and short-range proton-neutron correlations. It turns out that the summary rates of the two reactions are fairly insensitive to these effects. Using the sums one could extract capture states and neutron radii consistent with results obtained in other experiments. On the other hand, only a fraction of the antiproton capture results have been used for this purpose. There are other possibilities, more demanding on theories of nuclear structure which yield additional information.

2. Other possibilities

Two specific problems arise in this research:

(1) studies of few nucleon correlations at nuclear surfaces;
(2) information on the densities of excited nuclear states below the continuum threshold.

The first point represents a longstanding aim of nuclear physics, and has some chance to materialise. The experiments performed in nitrogen indicate effects of α particle correlations expected in the residual system formed in the antiprotonic captures. These could be visible, via double-pion exchange in final states, at the tails of the $P[Q]$ spectra. High experimental precision would be required for extraction of such effects.

The effect of proton-neutron nucleon short-range correlations is clearly visible in the $P[Q]$ distributions in medium and heavy nuclei. It changes $\pi^+ \to \pi^0$ and $\pi^- \to \pi^0$ transition rates in different ways, enhances $\lambda+$, and reduces λ^-. At the moment it presents the main stumbling block in our analysis. With more systematic studies of isotopic differences, the pionization data will be useful to study the density distribution of correlated p-n pairs.

The second point arises in the discussion of pion charge-exchange reactions. These processes are blocked by the Pauli principle. The effect is small as pions are very fast, nevertheless it matters in the analysis of $P[Q]$ and the extraction of capture orbits. In this work this question is circumvented to a certain extent. With more accurate experiments a detailed description would be a challenge but also an advantage.

TABLE XIV. Probabilities of multimeson state formation in antiproton-proton $MP[k]$ and antiproton-neutron $MN[k]$ annihilations, k is the number of $(\pi^+\pi^-)$ pairs.

$MP[k]$	$k=0$	$k=1$	$k=2$	$k=3$
At rest [18]	0.029	0.398(0.018)	0.527(0.017)	0.046(0.010)
Flight [17]	0.055 (20)	0.397(0.010)	0.500(0.011)	0.048(0.003)
At rest [17]	0.064 (4)	0.423(0.010)	0.469(0.011)	0.044(0.003)
$MN[k]$				
At rest [18]	0.0655	0.733	0.1893	0.0121
Flight [17]	0.184(0.008)	0.595(0.014)	0.217(0.009)	0.04(0.01)
At rest [17]	0.168 (8)	0.595(0.014)	0.230(0.009)	0.07(0.02)

PUMA offers additional values as it will detect detailed charge structure in each Q channel.

3. Requirements for higher precision

Three problems are met in this analysis:

(1) The hydrogen contamination should be well controlled.
(2) The ratio $R_{n/p}$ should be known with increased precision. $R_{n/p}$ is energy dependent and needs to be known in the subthreshold energy region. In this work, the Paris $\overline{N}$-N potential was used to generate it. It does well in the region of -30 MeV up to -15 MeV required for old experiments. However, PUMA intends to study chains of isotopes of fewer and fewer bound neutrons. That requires precise extension of $R_{n/p}$ into the region -15 until 0 MeV. This involves an update of the Paris or another $\overline{N}$-N interaction model.
(3) Emission rates of neutral pions in the $(\overline{p}n)$ annihilation should be better known.

ACKNOWLEDGMENTS

S.W. enjoyed the hospitality, profitable discussions, and help at Université Paris-Saclay and IJCLab Orsay.

APPENDIX A: PION MULTIPLICITY DISTRIBUTIONS IN $\overline{p}N$ ANNIHILATIONS

Below we list the charged and neutral pion multiplicities extracted from annihilation experiments [17–19]. Table XIV contains matrices $M[k]$ which give the probabilities of $k(\pi^+\pi^-)$ pairs emitted in a single annihilation event. In this work we use results obtained at rest in Ref. [18]. These are very close to the chamber measurements of Ref. [17] in the $\overline{p}p$ system but differ in the $\overline{p}n$ system. On the other hand the chamber results obtained in flight for antiproton momenta in the 0.25–0.47 GeV/c region are very close to those obtained at rest.

More detailed information on the probabilities to emit $k(\pi^+\pi^-)$ pairs and m π^0 mesons is collected in a matrix $M[k,m]$. It is more difficult to come by. The results used here are based upon scattering $\overline{p}d$ experiments at 1.09 GeV/c [19]. The basic $\overline{p}N \to$ mesons cross sections were measured in the dominant final-state channels and cross sections for less

TABLE XV. Probabilities of multimeson state formation in antiproton-proton annihilations $MP[k,m]$, k is the number of $(\pi^+\pi^-)$ pairs, m is the number of π^0 mesons. Results with error bars are proportional to experimental cross sections, results with no bars follow extrapolations made in Ref. [19]. Numbers in $MP[k=0,m]$ column are our estimates.

	$MP[0,m]$	$MP[1,m]$	$MP[2,m]$	$MP[3,k]$
$m=0$	0	0.061(0.003)	0.144(0.007)	0.285
$m=1$	0	0.150(0.017)	0.522(0.053)	0.628
$m=2$	0.2	0.349(0.016)	0.1807	0.083
$m=3$	0.5	0.333	0.1325	0
$m=4$	0.3	0.073	0	0
$m=5$	0	0.034	0	0

frequent events were obtained by extrapolations in terms of a model (see Ref. [19] for more details). We have added our own crude estimates of $M[k=0,m]$ which amount to a 5% of the total. The results given in Tables XV and XVI assume $M[k,m]$ to be proportional to the corresponding cross sections and normalized $\sum_m M[k,m]=1$ for each k. Pionization analysis requires precise data for the difference of charged and neutral meson emission probabilities, as indicated in Table XVII.

APPENDIX B: $R_{n/p}$ FROM PARIS POTENTIAL MODEL

Antiproton nucleon interactions involve S and P wave interactions. The rates of absorption are given by imaginary parts of the $p\bar{p}$ and $n\bar{p}$ scattering amplitudes A_i. These are determined by scattering length a_0 and scattering volumes a_1 for these two systems. In nuclear capture one has to average these over atomic and nuclear states and

$$A_i = \langle L, \text{valence}|[a_0(E) + 3\nabla a_1(E)\nabla]|L, \text{valence}\rangle \quad \text{(B1)}$$

separately for protons and for neutrons. The expectation value is calculated on the atomic function and on wave functions of valence nucleons. The basic quantities a_0, a_1 are the scattering length and scattering volumes averaged over spin states. The difficulty in this way is that nucleons are bound and E—the kinetic energy in the antiproton nucleon center-of-mass system—is negative. It is located below threshold due to the nucleon binding (separation) energy S_N, atomic binding B_A and recoil energy of the $N\bar{p}$ pair with respect to the residual

TABLE XVI. Probabilities of multimeson state formation in antiproton-neutron annihilations. See caption for Table XV. Numbers in $MN[0,m]$, $MN[3,m]$ columns are our extrapolations.

	$MN[0,m]$	$MN[1,m]$	$MN[2,m]$	$MN[3,m]$
$m=0$	0	0.061(0.003)	0.227(0.012)	0.2
$m=1$	0	0.324	0.453(0.020)	0.5
$m=2$	0.2	0.349 (0.015)	0.320(0.015)	0.3
$m=3$	0.5	0.196	0	0
$m=4$	0.3	0.068	0	0

TABLE XVII. The pion charge multiplicities $\langle n\rangle$ obtained in $p\bar{p}$ and $n\bar{p}$ annihilations.

	$\langle n^+\rangle$	$\langle n^-\rangle$	$\langle n^0\rangle$
$(p\bar{p})$	1.59 ± 0.05	1.59 ± 0.05	1.73 ± 0.07,
$(n\bar{p})$	1.148 ± 0.05	2.148 ± 0.05	1.80 ± 0.07

nucleus

$$E_{N\bar{p}} = M_N + M_{\bar{p}} - S_N - B_A - \frac{P_{cm}^2}{2(M_N + M_{\bar{p}})}. \quad \text{(B2)}$$

The subthreshold scattering amplitudes are calculated in terms of an effective $\widetilde{T}(r,E)$ matrix defined in the coordinate representation by

$$\widetilde{T}(r,E) = \frac{\mu_{N\bar{N}}}{2\pi} V_{N\bar{N}}(r,E) \frac{\Psi(r,E,k'(E))}{\psi_o(r,k'(E))}, \quad \text{(B3)}$$

with $k'(E) = \sqrt{2\mu_{N\bar{N}}E}$. In this equation, $\Psi(r,E,k'(E))$ is the solution of the Lippman-Schwinger equation $\Psi = \psi_o + G^+ V_{N\bar{N}}\Psi$ or of an equivalent Schrödinger equation, and $V_{N\bar{N}}$ is the Paris potential. The procedure, applied to all involved partial waves is described in detail in Ref. [10]. The results are presented in Fig. 1.

Nuclear calculations of A_i are messy because these involve high-l valence nucleon wave functions and high-L atomic states. However, the capture is peripheral and nucleons are beyond attractive nuclear potential. The shape of wave functions is determined by binding and the centrifugal plus Coulomb potentials. The nucleons involved are well beyond the classical turning point and WKB functions could be used. Calculations of A_p, A_n are performed via the gradient formula in the p waves as discussed in Ref. [10]. The recoil momenta P_{cm} involve high nucleon and high antiproton angular momenta. The calculations are fairly involved but are dominated by tangential components and are easier to control

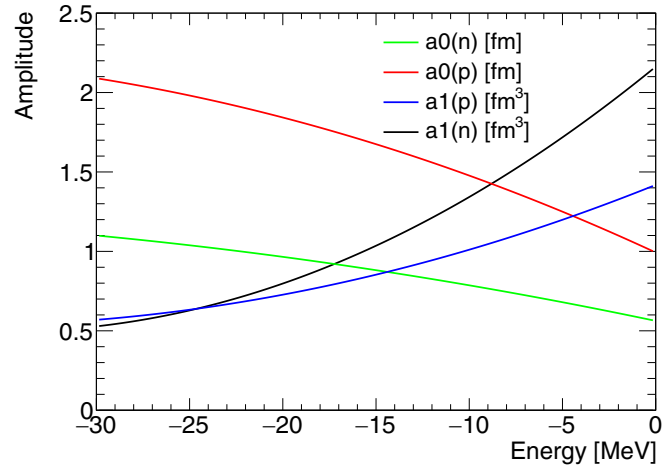

FIG. 1. Subthreshold, spin averaged $\bar{p}p$ and $\bar{p}n$ absorptive amplitudes calculated with Paris 09 potential. S waves in fm units and P waves in fm^3 units. With this solution the P-wave amplitudes are affected by the $^{33}P_1$ resonance at -4.8 MeV.

TABLE XVIII. $R_{n/p}$ calculated with the Paris 09 potential [9] for the dominant capture states.

	C	N	Ti	Ta	Pb
$R_{n/p}$	0.698	0.780	0.774	0.889	0.920
L_{dominant}	2	2	4	8	9

once the capture orbit is established. Amplitudes given by formula (B1) in the surface region are determined mainly by nuclear wave functions. Paris potential reproduces quite well the deuteron $R_{n/p} = 0.82$ and helium $R_{n/p} = 0.48$ data [10]. For loosely bound systems, with energies $E_{N\bar{p}}$ closer to the mass threshold the Paris potential predicts much stronger absorption on neutrons. Hence larger $R_{n/p}$ in deuteron. In large nuclei, with typical separation energies of 8 MeV and large angular momenta, the $R_{n/p}$ increases with the nuclear size.

Optical potentials usually assume or fit $R_{n/p}$ in the range 0.9–1.0 [23,24] and the same values were used for extraction of neutron haloes from capture experiments [14,21]. These, in particular in heavy nuclei, are close to the results obtained with the recent version of the Paris potential [9] displayed in Table XVIII. This potential generates a quasibound state in a P wave of not well established energy. The effect of this state on a quartet state amplitude is presented in Fig. 2 (figure taken from Ref. [10]). This wave is mainly responsible for the $R_{n/p}$ energy dependence in the subthreshold region. An analysis of light antiprotonic atoms [10] indicates that the position of the involved P wave resonance is expected to be about -10 MeV and not -4.8 MeV as predicted in Ref. [9] and shown in Fig. 2. It could enhance the calculated $R_{n/p}$ by a few percent and should be implemented before new experiments materialize.

APPENDIX C: PIONIZATION IN NUCLEAR CAPTURES OF ANTIPROTONS

Antiprotons circulating nuclei in atomic states are absorbed by the nucleus from high-angular-momentum states. At nuclear distances the repulsion due to centrifugal barriers makes

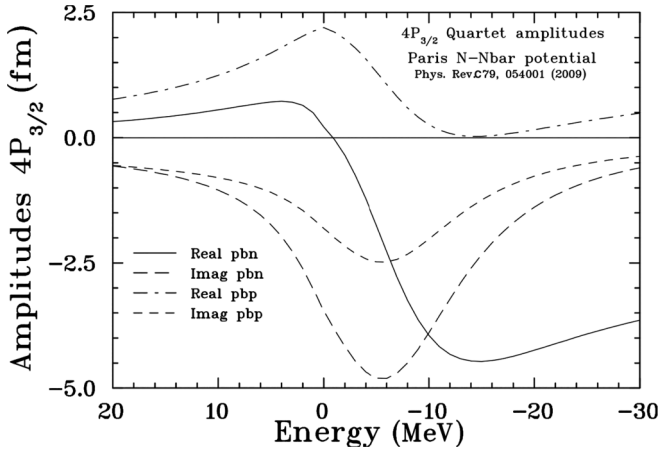

FIG. 2. Subthreshold, $\bar{p}p$, and $\bar{p}n$ amplitudes calculated with the Paris 09 [9] potential in $^{33}P_1$. This amplitude may be tested in measurements of fine-structure splitting in antiprotonic deuteron.

atomic wave functions fall down as $\Psi \sim r^L$ where r is the radial coordinate and L is the angular momentum. This makes nuclear captures happen at distant peripheries, typically at less than 5% of the central nuclear density.

Antiproton annihilation and related emission of mesons is a complicated quantum process. Approximations are necessary. Let us outline these in the limit of zero range annihilation. Extensions to finite ranges will be introduced later in the way shown in Ref. [15]. The basic transition matrix element for the pionization is

$$f = \langle \Psi_\pi \Psi_{A-1} | t_{\bar{p}N\to M} | \Psi_A \psi_L \rangle, \tag{C1}$$

where Ψ are wave functions of a final $A-1$ state and the initial A nuclei, ψ_L is the atomic wave function of antiproton in a state of angular momentum L and Ψ_π is the wave function of the final-state mesons. First, we assume that the initial step of the $\bar{p}$ annihilation is localized on a single nucleon. Annihilation on two nucleons—the Pontecorvo reaction—amounts to a fraction of 0.5(1)% events in helium [12]. Given that the helium nucleus is very dense, this fraction may be expected to be an upper limit. We stay with the single nucleon captures and single-particle nuclear models of nuclei until the data require changes. One consequence is that $\langle \Psi_{A-1} | \Psi_A \rangle = \varphi_n(r)$ where φ_n is a nuclear wave function of the struck nucleon. The transition element reduces to

$$f = \int d\mathbf{r} \prod_i \overline{\Psi_\pi^-}(\mathbf{r}) t_{\bar{p}N\to M} \psi_L(r) \varphi_n(r), \tag{C2}$$

where φ_n is a function of the struck nucleon and $t_{\bar{p}N\to M}$ is an operator for the transition of the $\bar{p}N$ system into mesons. The mesonic wave function Ψ_π is given by a product of single meson waves ϕ_i of momenta $\mathbf{k}_i$

$$\Psi^\pi = \prod_i \overline{\phi^-}(\mathbf{r}, \mathbf{k}_i). \tag{C3}$$

All functions ϕ^- involve final-state interactions. The mesons are formed on the nuclear surfaces and propagate in all directions. Average mesonic momenta are large $k \approx 400$ MeV/c and allow for eikonal description. Wave functions for each outgoing pion are thus given by

$$\overline{\phi^-}(\mathbf{r}, \mathbf{k}) = \exp\left[i\mathbf{r}\mathbf{k} - iS(\mathbf{r}, \mathbf{k})\right], \tag{C4}$$

$$S(\mathbf{r}, \mathbf{k}) = \int_0^\infty ds[\sqrt{k^2 - U(\mathbf{r} - s\hat{\mathbf{k}})} - k], \tag{C5}$$

where U is the potential describing absorption, elastic, and inelastic scattering. Coordinate $\mathbf{r}$ refers to the nuclear center. Boundary conditions are set in such a way that

$$T(\mathbf{r}, \mathbf{k}) = |\phi^-(\mathbf{r}, \mathbf{k})|^2 = \exp\left[-2\mathrm{Im}S(\mathbf{r}, \mathbf{k})\right] \tag{C6}$$

gives the transmission probability for a meson emitted at point $\mathbf{r}$ in the direction of momentum $\mathbf{k}$. The loss of mesonic flux is determined by ImU which by unitarity is related to the relevant cross sections.

To obtain the rate of decay into mesons, amplitudes (C2) are squared $f\overline{f}$ and summed over the initial nucleons and final pions states of interest. Next, the sum is integrated over the phase space.

The high mesonic momenta allow one to present the mesonic wave and amplitude f as a function of the total momentum of all mesons $\mathbf{P} = \sum \mathbf{k}_i$ which equals the recoil momentum of the residual nucleus. In addition, the large mass excess in the initial $\overline{p}N$ channel allows us to use closure over the final nuclear states. This approximation simplifies the internal part of the $f\overline{f}$ expression integrated over the final phase space,

$$\int d\mathbf{P} dL^{\text{c.m.}} \exp[-i(\mathbf{r}-\mathbf{r}')]\delta(E^{\text{ini}} - E(P) - E^{\text{c.m.}}) \approx (2\pi)^3 \delta_\epsilon(\mathbf{r}-\mathbf{r}') \int dL^{\text{c.m.}} \delta(E^{\text{ini}} - E^{\text{c.m.}}). \quad \text{(C7)}$$

The phase-space element factorizes into total momentum part and an internal part $L^{\text{c.m.}}$. Formula (C7) contains conservation of the initial energy $E^{\text{ini}} \simeq 2M$ and the final energy of emitted mesons in their center of mass system corrected for recoil energy $E(P)$. The E^{ini} is large while the recoil energy $E(P)$ is small and the total phase-space dependence on $E(P)$ is very weak. For decays into n mesons one has

$$\int dL^{\text{c.m.}} \delta(E^{\text{ini}} - E(P) - E^{\text{c.m.}}) \sim [E^{\text{ini}} - E(P)]^{2n-1}. \quad \text{(C8)}$$

This energy dependence inserted into equation (C7) generates some spread of the "true" $\delta(\mathbf{r}-\mathbf{r}')$ denoted above by δ_ϵ. With an average $n \simeq 5$ the smearing of the δ_ϵ singularity amounts to about 0.2 fm. We neglect it as this radius is much smaller than 1 fm range characteristic for annihilation processes. The last approximation allows us to express the decay rates in terms of the atomic and nuclear density overlaps

$$\Gamma = \int d\mathbf{r} |\psi_L(r)|^2 \Sigma_n |\varphi_n(r)|^2 \int dL^{\text{c.m.}} |t_{\overline{p}N\to M}|^2 T(\mathbf{r}, \mathbf{k}). \quad \text{(C9)}$$

The second integral is calculated in the limit of no final-state interaction and up to a normalization constant equivalent to probabilities M introduced in the main text. Given that there is no reliable theory to calculate $t_{\overline{p}N\to M}$ we rely upon the experimental values. On the other hand, with the method to study $P[Q]$ developed in the main text we need to calculate only the relative rates of *single* meson emissions. These are given by simpler expressions

$$T_\alpha = \int d\mathbf{r} \frac{|\psi_L(r)|^2 \Sigma_n |\varphi_n(r)|^2}{\Theta} \left[\int dL^{\text{c.m.}} T_\alpha(\mathbf{r}, \mathbf{k}) \right], \quad \text{(C10)}$$

$$\Theta = \int d\mathbf{r} |\psi_L(r)|^2 \Sigma_n |\varphi_n(r)|^2, \quad \text{(C11)}$$

where α denotes π^+, π^-, π^0. The average transmission T_α is calculated with the nuclear potential corresponding to the specified meson. Formula (C10) may be used to calculate the total effect of all modes of final absorption: two nucleon absorptions and charge exchanges. To calculate effects of a selected specific mode we will use a simplified form of formula (C9) to be discussed later.

The region of nucleus studied in antiproton capture is given predominantly by atomic and nuclear density overlaps

$$\Theta(r) = |\psi_L(r)|^2 \Sigma_n |\varphi_n(r)|^2 \equiv |\psi_L(r)|^2 \rho(r), \quad \text{(C12)}$$

where the density ρ generated by the sum of single nucleon densities may be the proton or neutron density. As discussed in the main text, the densities involved should include a folded range of the absorption. However, the qualitative picture described below is not much different. The $\Theta(r)$ is significant in a spherical shell with a radius $R_c \approx c + \delta$, where c is a half density nuclear radius and $\delta \simeq 1.5$ fm [31]. Antiproton absorption experiments weight this region by the chances to transmit the final waves. At very large distances, $T(r)$ given by formula (C6) approaches unity, thus final interactions suppress the internal part of $\Theta(r)$. The strongest suppression happens with the radiochemical experiments that detect cold final nuclei. Hence, the halo factors measured in these experiments are larger than the halo factors obtained in the pionization experiments. The experience of x-ray measurements shows that radiochemical results are determined predominantly by captures from the "upper" levels [15] while the pionization results are determined by captures from a mixture of "upper" and "lower" levels.

In the next section we discuss the two main absorption modes which determine spectra of final mesonic charges.

1. True two-nucleon absorptions

Optical potentials for π mesons at the high momentum of interest are not well known. Fortunately, Johnson and Satchler [32] offer an optical potential description of $\pi^\pm$ scattering on Pb at kinetic energy $T_\pi = 291$ MeV, approximately at the center of the meson energies allowed in the antiproton captures. This potential contains also a component due to two-nucleon capture. The Klein Gordon equation for mesonic wave function involves, in general, s and p wave interactions,

$$[-\Delta - k^2 + U_s + \overrightarrow{\partial}\, U_p \overrightarrow{\partial}\,]\phi = 0. \quad \text{(C13)}$$

Under conditions that the momentum k is large and the potential is not changing too rapidly, one obtains rapid expansion of $S(k, r)$ in terms of k^{-1}. Usually the first term in this expansion gives satisfactory results. This unfortunately is not the case for the gradient potential, and higher-order corrections have to be introduced. In these circumstances it is easier to perform the Krell-Ericson [33] transformation

$$\phi = \psi/\sqrt{1 - U_p(r)}, \quad \text{(C14)}$$

which generates

$$[-\Delta - k^2 + U_l]\psi = 0, \quad \text{(C15)}$$

with a local potential [32]

$$U_l = \frac{U_s - k^2 U_p}{1 - U_p} - \frac{\overrightarrow{\partial}\, U_p \cdot \overrightarrow{\partial}\, U_p}{4(1-U_p)^2} - \frac{\Delta U_p}{2(1-U_p)}. \quad \text{(C16)}$$

We need two nucleon term U_{NN} which involves a part of the Kisslinger term U_p. Its semiphenomenological form

$$U_{NN} = 4\pi \left[4\rho_n \rho_p C_0 \mp \left(\rho_n^2 - \rho_p^2 C_1\right)\right] \frac{1}{1 + E_\pi/2M_n} \quad \text{(C17)}$$

was used in Ref. [32] with best-fit parameters $C_0 = 1.0406 + i1.4690$ fm^6 and $C_1 = -0.8569 - i0.1856$ fm^6. The upper

TABLE XIX. Two-nucleon capture parameters ω_{NN} calculated for a limited two-nucleon only absorption model. Second line follows optical potential from Ref. [32]. As ω^+ and ω^- differ as little as 1.5% we give average of the two. Third line follows extended method from Ref. [34]. L are the angular momenta of the dominant capture orbits.

Pb	Ta	Ti	N	C
$L = 8$	8	4	2	2
0.309	0.251	0.253	0.208	0.186
0.311	0.297	0.238	0.197	0.175

sign corresponds to π^+ and the lower to π^-. The advantage of this parametrization is that it was tested in a heavy nucleus, the disadvantages are that the optical potential is tested upon total pion-nucleus cross sections and it offers no analytic form of its energy dependence. The chance for a single charged meson to avoid two nucleon absorptions is given by equations (C6) and (C10) and presented in Table XIX.

For comparison, we turn to another, theoretically motivated, energy-dependent two-nucleon capture approach. The general understanding is that the U_{NN} term describes two nucleon capture initiated by the excitations of $\Delta(1233)$. A direct model of such potential was offered by Muttaz Nuseirat *et al.* [34] and later by Alquadi and Gibbs in Ref. [35]. This potential is local

$$\mathrm{Im}U_{NN} = -\lambda_o \frac{(\Gamma/2)^2}{(E_o - E_\pi)^2 + (\Gamma/2)^2}\rho(r)^2, \tag{C18}$$

with parameters $\lambda_o = 46.35$ fm^4, $E_o = 215$ MeV, and $\Gamma = 77$ MeV. These parameters were tested in light nuclei and for pion kinetic energies $T_\pi < 180$ MeV/c, in $Z = N$ situations. No real part is suggested, as might be expected for high-energy-transfer reactions.

To compare the two methods we extend formula (C18) to neutron excess nuclei in the way used in Ref. [32], that is, $(\rho_n + \rho_p)^2 \to 4\rho_n\rho_p$. We also need extension to higher energies to cover the right shoulder od $\Delta(1233)$. This requires a change of the width and $\Gamma = 100$ MeV is used. This choice follows analysis of another experiment by the same group, and we extract it from Fig. 2 in Ref. [35]. The experimental width of free $\Delta(1233)$ measured in charge exchange scattering is a bit larger $\Gamma = 110$ MeV [36]. Numerical comparison of the two approaches is given in Table XIX which shows average NN absorbtion strengths ω_{NN} for several nuclei. These calculations were performed with $\Theta(r)$ determined by charge density and the extrapolated potential for two nucleon capture from Ref. [35]. It turns out that the two methods of calculation yield fairly close results (with the exception of Ta). Both approaches are essentially the same for π^+ and π^- and we extend them also to the π^0 case. This comparison shows a fair reliability of the true absorption description. This calculation is of limited significance anyway. We show in next sections that ω_{NN} is strongly suppressed by the competing charge exchange and the uncertainties become insignificant.

2. Charge-exchange processes

The pion charge-exchange reaction

$$\pi^- p \to \pi^0 n \tag{C19}$$

was studied up to 250 MeV pion kinetic energies [36]. The cross section follows the shape of $\Delta(1233)$ which dominates the reaction and may be parameterized by

$$\sigma_{\mathrm{expt}} = 48.1 \frac{(\Gamma/2)^2}{(\Gamma/2)^2 + (T_\pi - T_r)^2}\ \mathrm{mb}, \tag{C20}$$

where $T_r = 176$ MeV and the width at the resonance is 110 MeV. The resonant profile was extrapolated to 300 MeV by SAID [36] and we extrapolate it further by some 50 MeV. The experimental profile and both extrapolations into the interesting region of $T_\pi > 200$ MeV require a weak increase of the width. On the distant right shoulder of Δ our extrapolation follows $\Gamma = 70 + T_\pi/10$ MeV.

Reaction (C19) is an inverse of reaction (6). By the isospin symmetry these two differ only slightly, by the final phase space. Hence, equation (C20) describes also other charge-exchange reactions. The transmission probability T_{expt} for the meson formed at point $\mathbf{r}$ to leave the nucleus with the primary charge is now calculated with the standard expression for the inverse charge-exchange length $\lambda_{\mathrm{expt}} = \sigma_{\mathrm{expt}}\rho_p(r)$ where ρ_p is the proton density.

$$T_{\mathrm{expt}}(\mathbf{r}, \mathbf{k}) = \exp\left[-\lambda_{\mathrm{expt}} \int_0^\infty ds \rho_p(\mathbf{r} - s\widehat{\mathbf{k}})\right]. \tag{C21}$$

The coordinate $\mathbf{r}$ refers to the nuclear center and $\mathbf{k}$ is the pion momentum in the nuclear c.m. system. For comparison with the true pionic capture we define $U_{\mathrm{expt}} = \lambda_{\mathrm{expt}}k$ which has the dimension of fm^{-2}. Similar expressions hold also for $\pi^+ n$ charge exchange. Similarly to the true absorption T_{expt} is averaged over mesonic energies and flight directions. The chance for a charge meson to avoid charge exchange is again given by Eqs. (C6) and (C10).

Kaufmann and Gibbs [37] noticed strong Pauli blocking of charge exchange reaction in nuclear matter. This reference calculates charge-exchange process leading to a definite final nucleus below the neutron emission threshold. Cross sections obtained in this way amount to about one mb. On the other hand total charge-exchange cross sections measured by Ashery *et al.* [38] reach hundreds of mb. Thus our phenomenological exchange parameters $\lambda^\pm$ are essentially due to high nucleon excitations permitted by the exclusion principle. To account for that we use a simple Fermi gas model and calculate a blocking factor $B(r, \mathbf{k}, \mathbf{k}_n)$ defined as the ratio of allowed us to the total phase space for a given pion and nucleon momenta at a nucleon position at distance r. Next this quantity is averaged over nucleon momenta k_n allowed by local Fermi gas model and the average is denoted by $B(r, k)$. The actual cross section, entering Eq. (C21) is now related to the experimental one via

$$\sigma_{\mathrm{expt}}^{\mathrm{block}} = B(k, r)\sigma_{\mathrm{expt}}. \tag{C22}$$

Additional assumptions are made for the lowest values of the limiting blocking energies. For final neutrons in light nuclei (C, N, Ti) the density of excited levels is low and

we assume blocking of final neutron states up to the neutron separation energy. However, in heavy nuclei (Ta, Pb) the density of excited states is large and the blocking limit assumed is the Fermi energy. For protons, the final states are blocked up to top of the Coulomb barrier reduced by 1.5 MeV. The latter reduction takes into account the time used for measurements assumed to be about 1 second. A simple model for Coulomb penetration (e.g., Ref. [39]) finds that, for standard outgoing wave, the internal wave function is negligible below this energy. In principle, Gamov states might arise, but the accompanying pions have no definite energies due to strongly absorptive nuclear medium. In such circumstances the formation of Gamov states suffers dramatic suppression.

We find the blocking effect to reduce the calculated Λ^+ by about 10% and Λ^- by about 30% in high Z nuclei. As shown in Sec. III average values of parameters $\Lambda^+ + \Lambda^-$ obtained from the phenomenological analysis and the calculated values are in good agreement. However the difference $\Lambda^+ - \Lambda^-$ is not reproduced. This question is discussed in the next section.

3. Relation of charge loses to charge gains

Reactions of charge loss due to charge exchange $\pi^\pm \to \pi^0$ run parallel to the true meson absorption. The two modes of absorption compete to reduce the charged pion flux. This effect is implemented into eikonal description (C7) adding two complex potentials representing the two modes. Thus for the π^+ loss one has

$$U_{\rm loss}(\pi^+) = U_{NN} + U_{\rm expt}(\pi^+ \to \pi^0). \tag{C23}$$

It leads to the total loss probability, denoted by $\omega^+_{\rm tot}$, which is calculated in the same manner as ω_{NN} but with full potential $U_{\rm loss}(\pi^+)$. The two-nucleon potential of Eq. (C18) is used.

Calculation of charge gains due to $\pi^0 \to \pi^+$ is more difficult. First we calculate the total loss of a neutral meson flux due to three competing processes and denoted by $\omega^0_{\rm tot}$. The relevant potential is

$$U_{loss}(\pi^0) = U_{NN} + U_{\rm expt}(\pi^0 \to \pi+) + U_{\rm expt}(\pi^0 \to \pi^-). \tag{C24}$$

The two-nucleon capture contribution is the same as that used for charged mesons. From the total loss rate $\omega^0_{\rm tot}$ one needs to select the part due to $\pi^0 \to \pi+$. This part denoted by $P^+\omega^0_{\rm tot}$ generates the gain in the π^+ channel. To obtain the net absorption of π^+ mesons denoted by Ω^+ we need to subtract

$$\omega^+_{\rm tot} - P^+\omega^0_{\rm tot} = \Omega^+. \tag{C25}$$

The relevant fraction P^+ of the exchange process rate is calculated from a standard decay formula. We pick up the second piece of integral related to equation (C9):

$$\Gamma = \int d\mathbf{r}\left[\int dL^{\rm c.m.} T_\alpha(\mathbf{r},\mathbf{k})\right][U_{NN} + U_{\rm expt}(\pi^0 \to \pi+) + U_{\rm expt}(\pi^0 \to \pi^-)]|\Psi_L(r)|^2\rho(r)T(r), \tag{C26}$$

and divide by the sum of all three terms. Equations analogous to (C25) and (C26), used to obtain Ω^+, are used again to obtain Ω^-.

The relative strengths of the three potentials in Eq. (C26) are indirectly related to the absorption and charge-exchange cross sections on nuclei which are of comparable magnitudes [38]. On the other hand, antiproton absorptions from atomic states enhance the surface interactions that is charge exchanges linear in the nuclear density ρ against the two-nucleon absorptions linear in ρ^2. Thus the latter is at a disadvantage. To summarize this section we stress that equation (C25) is the most sensitive point of this calculation. In a fairly involved way it subtracts rates of direct- and charge-exchange processes. These rates differ mostly by the density of the initial nucleons and blocked phase space allowed us to final nucleons. As it is a difference between two quantities it accumulates uncertainties of the two basic components. A way to improve accuracy is to use sums $\Omega^- + \Omega^+$ which in a way averages over initial proton and neutron numbers and at the same time over the final proton blocking and neutron blocking. The latter point is significant. One needs to describe both neutron and proton spectra in a consistent and related way. With the Fermi gas model used here it is prudent to discuss sums $\Omega^+ + \Omega^-$ and $\Lambda^+ + \Lambda^-$ to reduce the effect of model simplicities. An additional argument for such procedure is given in Sec. C 5 where we discuss proton-neutron correlations.

4. Correlations at nuclear surfaces

The nitrogen experiment discussed in Sec. III B finds a sizable fraction of final $Q = 3$ and $Q = -3$ charges. It is not reproduced by the mechanism developed so far and apparently it is due to strong few nucleon correlations. Being sizable in nitrogen, weaker in carbon and not noticeable in heavier nuclei, it indicates a predominant role of α-particle correlations. This possibility is studied below.

Double π charge exchange of the type $\mathrm{He}(\pi^+,\pi^-)X$ is a rare process. Kinnock *et al.* find it also strongly energy dependent [40], at kinetic energy $T = 180$ MeV the total cross section $\sigma_{cc} = 489(23)$ μb and rises linearly to 1460(105) μb at $T = 270$ MeV. We extrapolate it linearly up to $T = 400$ MeV, where σ_{cc} becomes 2800 μb. Similar measurements taken in oxygen [41] indicate that the total cross section scales as the four α-particle structure expected in this nucleus. We follow that and assume that, in nitrogen, the initial antiproton capture takes place at a valence proton (or neutron) and the residual nucleus is predominantly a 3α system. The double charge-exchange rate is introduced in a way analogous to the single charge-exchange parameters $\lambda^\pm$. It is denoted λ_{--} because it changes the initial total mesonic charge Q by two units. Next, $\lambda_{--} = 1 - T_{cc}$, where, following Eq. (C21), the chance $T_{cc}(r)$ for the meson formed at point r to leave the nucleus and avoid double charge-exchange is given by

$$T_{cc}(\mathbf{r},\mathbf{k}) = \exp\left[-\sigma_{cc}(T)\int_0^\infty ds\rho_{3\alpha}(\mathbf{r} - s\widehat{\mathbf{k}})\right]. \tag{C27}$$

In this expression σ_{cc} is the cross section for double charge exchange on a free α particle, the coordinate $\mathbf{r}$ refers to the nuclear center, and $\mathbf{k}$ is the pion momentum in the nuclear c.m. system. Density, in this case, is the density of three α

particles. We assume that centers of the alpha particles are located in a volume of Gaussian profile with a R_{ms} radius chosen so that $R_C^2 = R_{ms}^2 + R_\alpha^2$ where the R_C is the charge radius of carbon and R_α is the charge radius of the α particle. The T_{cc} of equation (C27) is averaged over the meson momenta and the initial antiproton density in the capture orbit. The averaged parameter $\lambda_{++} = 1 - \langle T_{cc}\rangle$ calculated for $\pi^+ \to \pi^-$ (and the same for $\pi^- \to \pi^+$) is put as an *additional* term into the initial scheme which determines our ω and σ. With the initial $p\bar{p}$ annihilation beginning with $Q = 0$ the double charge-exchange process enhances the rate in $Q = 3$ channel by

$$\Delta P[3] = \sum_{k\geqslant 2,m} MP[k]MP[k,m](T^+\omega^-)(T^+\lambda^{++}) \times (T^+T^-)^{k-2}, \tag{C28}$$

which corresponds to annihilation of one π^- meson and the double charge exchange of another π^- meson. The same $Q = 3$ channel may be populated by double charge exchange and a single $\pi^- \to \pi^0$ transformation. One has an additional way to reach $Q = 3$

$$\Delta P[3] = \sum_{k\geqslant 1,m>0} MP[k]MP[k,m]\lambda^+(T^+\lambda^{++})(T^+T^-)^{k-1}, \tag{C29}$$

and contributions from first order λ^{++} which lead to the $Q = 2$ channel. In the primary capture on neutron, λ^{--} adds directly to the final $Q = -3$ channel. Parameters $\lambda^{++} = \lambda^{--} = 0.03$ obtained in this way are much smaller than the main $\lambda \approx 0.25$. Still, the inclusion of double charge exchange considerably improves the fit, although it falls below the experimental values in $|Q| = 3$ sectors. The results are given in Table XIII of the main text.

5. Short-ranged *p-n* correlations

High-energy electron scattering on nuclei finds large momentum components in nucleon wave functions. These are attributed to short-range proton-to-neutron correlation. The enhancement of *n-p* correlations over *p-p* correlations is particularly strong in heavy nuclei [42]. Calculations [43] indicate that about 20% of single nucleon momentum spectra in nuclei are due to these proton-neutron correlations. The latter cover momenta in the 1.5–3.5 fm^{-1} region sizably above the Fermi momentum. This finding is indirectly but clearly seen in nuclear antiproton capture.

Charge-exchange reactions are blocked by the exclusion principle. To change sign in $\pi^0 p \to \pi^+ n$ reaction the neutral pion has to excite the neutron above the Fermi level. This blocking reduces the reaction rate by a 10%. In collisions $\pi^0 n \to \pi^- p$ the final proton has to be excited above the Coulomb barrier. This blocks the reaction rate by some 30% in heavy nuclei. A π meson colliding with a correlated pair encounters a high-momentum nucleon which has a better chance to be ejected above the Fermi level (or the Coulomb barrier). On the other hand it is a three body process and to materialize it both nucleons have to be ejected. There are four reactions contributing to charge exchange, these are listed below and denoted by $\Delta()$. These affect $\Lambda^\pm$ parameters which give fractions of $\pi^\pm$ mesons formed in $\pi^0 \to \pi^\pm$ reactions:

TABLE XX. Pb atom. Pion charge-exchange parameters. The $\lambda^\pm$ are obtained from the best fit to experimental data presented in Table VIII. Numbers $\Lambda(l)$ are calculated in a simple single-particle nuclear model, for the two most likely atomic capture orbits. l are the angular momenta of these atomic states indicated by x-ray measurements. The real capture happens from a mixture of $l = 9$ and $l = 8$ states.

	$\Lambda(l=9)$	λ fitted to data	$\Lambda(l=8)$
λ^+	0.263	0.41(.03)	0.309
λ^-	0.234	0.14(0. 01)	0.248
$\lambda^- + \lambda^+$	0.497	0.55(.03)	0.55

$$\Delta\Lambda^+ = \Delta(\pi^0 p, n \to \pi^+ n, n) - \Delta(\pi^+ p, n \to \pi^0 p, p), \tag{C30}$$

$$\Delta\Lambda^- = \Delta(\pi^0 p, n \to \pi^- p, p) - \Delta(\pi^- p, n \to \pi^0 n, n), \tag{C31}$$

where the spectator nucleons are separated by commas. If one calculates $\Lambda^\pm$ the quantities $\Delta\Lambda$ are corrections to the rates obtained in a single-particle nuclear model. The corrections are due to nucleon momenta exceeding the Fermi momenta. The reactions Δ listed above involve direct and inverse charge-exchange reactions. One can see that the correction is positive in the Λ^+ case and negative in the Λ^- case, the result of enhanced proton blocking due to the Coulomb barrier.

Table XX shows that the calculated single-particle values for Λ^+ should be enhanced and the values for Λ^- should be reduced. *Such changes follow from the short-range correlations.*

A proper calculation of the expected effects is not simple as both nuclear and mesonic ingredients of the reactions involved are not certain. For the main purpose of PUMA—the extraction of neutron haloes—the procedure is much simpler. One notices that in the bulk of a nucleus the sum $\Delta\Lambda^- + \Delta\Lambda^+$ cancels to zero. Thus the single-particle model results for $\Lambda^- + \Lambda^+$ are sufficient to reach consistency with the best fit $\lambda^- + \lambda^+$. Then one proceeds with the extraction of capture orbits and neutron haloes.

On the other hand precise experimental determination of the charge spectra $P[Q]$ and systematic calculations of $\Delta\Lambda$ may present an added value to the PUMA experiment. In addition to the thickness of neutron haloes it may tell the densities of short correlations at nuclear surfaces. The effect of N-N' correlations is predominantly kinematic. The charge exchange becomes a three-body process between π, N, and N'. The characteristic feature of three-body Faddeev equations is that the energy of the π, N subsystem is reduced by the recoil energy of the other nucleon N'. Thus in the resonance formula (C20) the resonant energy $T_r = 176$ MeV is effectively pushed up by the recoil energy. In effect the resonant peak in pion-deuteron scattering is formed and

observed at $T_D \simeq 200$ MeV [44]. This kind of apparent Δ resonance shift makes significant changes in understanding of the pion charge exchange. The average pion kinetic energy $T_\pi \simeq 290$ MeV is much higher than the Δ position and the N' recoil moves the energy of π, N subsystem down closer to the Δ. Rykebush [43] calculations find an average momentum component due to N-N' short-range correlations to be about 2 fm^{-1} and this generates about 80 MeV recoil energy. Such a shift makes tremendous enhancement of the charge-exchange cross section (by a factor of three) and sizably changes the Λ values.

Our crude estimate based on high nucleon momentum component calculated in Ref. [43] and spatial distribution of short-range correlations analyzed in terms of Wigner matrix performed in Ref. [45] and in a nuclear model [46] allows two conclusions:

(1) The magnitudes of $\Delta\Lambda$ may well reach 20% corrections to the basic single nucleon model Λ.
(2) The reactions of interest are different on nuclear surface in particular on the surface of neutron excess nuclei. Orbital antiproton is captured predominately on a peripheral neutron. If it is a correlated neutron the emitted neutral meson undergoes $\pi^0 p \to \pi^+ n$ on a strongly correlated nearby proton, which is not blocked as the proton momentum is large. An estimate gives the dominant $\Delta\Lambda^+ \simeq 0.01$ in Pb nucleus, small but perhaps noticeable.

The pion charge exchange on correlated p-n pairs is an interesting problem which requires precise calculations. If performed, the PUMA experiments may add valuable data.

[1] D. H. Wilkinson, Nucleon clusters in the nuclear surface, Philos. Mag. **4**, 215 (1959).
[2] E. H. S. Burhop, Mesonic atoms, *High Energy Physics* (Acad. Press., New York, 1969), Vol. III, p. 109.
[3] A. Trzcinska *et al.*, Information on antiprotonic atoms and nuclear periphery from the PS209 experiment, Nucl. Phys. A **692**, 176 (2001).
[4] L. E. Agnew, T. Elioff, W. B. Fowler, R. L. Lander, W. M. Powell, E. Segrè, H. M. Steiner, H. S. White, C. Wiegand, and T. Ypsilantis, Antiproton interactions in hydrogen and carbon below 200 MeV, Phys. Rev. **118**, 1371 (1960).
[5] M. Wada and Y. Yamazaki, Technical developments toward antiprotonic atoms for nuclear studies of radioactive nuclei, Nucl. Instrum. Methods Phys. Res., Sect. B **214**, 196 (2004).
[6] T. Aumann, W. Bartmann, O. Boine-Frankenheim *et al.*, PUMA, antiproton unstable matter annihilation, Eur. Phys. J. A **58**, 88 (2022).
[7] F. Balestra, S. Bossolasco, M. P. Bussa, L. Busso, L. Fava, L. Ferrero, D. Panzieri, G. Piragino, F. Tosello, G. Bendiscioli, A. Rotondi, P. Salvini, A. Zenoni, Y. A. Batusov, S. A. Bunyatov, I. V. Falomkin, F. Nichitiu, G. B. Pontecorvo, M. G. Sapozhnikov, V. I. Tretyak, C. Guaraldo, A. Maggiora, E. Lodi Rizzini, A. Haatuft, A. Halsteinslid, K. Myklebost, J. M. Olsen, F. O. Breivik, T. Jacobsen, and S. O. Sorensen, Annihilation of antiprotons at rest in ^{3}He and ^{4}He, Nucl. Phys. A **474**, 651 (1987).
[8] R. Bizzari, P. Guidoni, F. Marcelija, F. Marzano, E. Castelli, and M. Sessa, Anti-proton-deuteron low-energy cross-section, Nuovo Cimento A **22**, 225 (1974).
[9] B. El-Bennich, M. Lacombe, B. Loiseau, and S. Wycech, Paris $N\bar{N}$ potential constrained by recent antiprotonic-atom data and $\bar{n}p$ total cross sections, Phys. Rev. C **79**, 054001 (2009).
[10] B. Loiseau and S. Wycech, Extraction of baryonia from the lightest anti-protonic atoms, Phys. Rev. C **102**, 034006 (2020).
[11] E. Klempt, C. Batty, and J.-M. Richard, The nucleon-antinucleon interaction at low energy: Annihilation dynamics, Phys. Rep. **413**, 197 (2005).
[12] G. Bendiscioli and D. Kharzeev, Antiproton-nucleon and antiproton-nucleus interaction, review of experimental data, Riv. Nuovo Cimento **17**, 1 (1994).
[13] M. Leon and R. Seki, Atomic Capture of Negative Mesons, Phys. Rev. Lett. **32**, 132 (1974).
[14] R. Schmidt *et al.*, Nucleon density of ^{172}Yb and ^{176}Yb at the nuclear periphery determined with antiprotonic x rays, Phys. Rev. C **58**, 3195 (1998).
[15] S. Wycech, J. Skalski, R. Smolanczuk, J. Dobaczewski, and R. J. Rook, Antiprotonic studies of nuclear neutron haloes, Phys. Rev. C **54**, 1832 (1996).
[16] W. M. Bugg, G. T. Condo, E. L. Hart, H. O. Cohn, and R. D. McCulloch, Evidence for a Neutron Halo in Heavy Nuclei from Antiproton Absorption, Phys. Rev. Lett. **31**, 475 (1973).
[17] T. E. Kalogeropoulos and G. S. Tzanakos, Total and partial $\bar{p}d$ cross sections from 0.26 to 0.47 GeV/c, Phys. Rev. D: Part. Fields **22**, 2585 (1980).
[18] J. Riedlberger, C. Amsler, M. Doser, U. Strauman, P. Truol, D. Bailey, S. Barlag, U. Gastaldi, R. Landua, S. Sabav, K. D. Duch, M. Heel, H. Kalinowsky, F. Kayser, E. Klempt, B. May, O. Schreiber, P. Weidenauer, M. Ziegler, W. Dahme, F. Feld-Dahme, U. Schaefer, W. R. Wodrich, S. Ahmad, J. C. Bizot, B. Delcourt, J. Jeanjean, H. Nguyen, N. Prevot, E. G. Auld, D. A. Axen, K. L. Erdman, B. Howard, R. Howard, B. L. White, M. Comyn, G. Beer, G. M. Marshall, L. P. Robertson, M. Botlo, C. Laa, and H. Vonach, Antiproton annihilation at rest in nitrogen and deuterium gas, Phys. Rev. C **40**, 2717 (1989).
[19] P. D. Zemany, J. M. Muntz, and Z. Ming Ma, Analysis of double-scattering mechanism in the $\bar{p}$d annihilation process between 1.09 and 1.43 GeV/c, Phys. Rev. D: Part. Fields **23**, 1473 (1981).
[20] M. Wade and V. G. Lind, Ratio of antiproton annihilation on neutrons and protons in carbon for low energy and stopped antiprotons, Phys. Rev. D: Part. Fields **14**, 1182 (1976).
[21] P. Lubinski, J. Jastrzebski, A. Trzcinska, W. Kurcewicz, F. J. Hartmann, R. Schmid, T. von Egidy, R. Smolanczuk, and S. Wycech, Composition of nuclear periphery from antiproton absorption, Phys. Rev. C **57**, 2962 (1998).
[22] G. Fricke *et al.*, Ground state nuclear charge distributions from electromagnetic interactions, At. Data Nucl. Data Tables **60**, 177 (1995).
[23] E. Friedman and A. Gal, In medium nuclear interactions of low energy hadrons, Phys. Rep. **452**, 89 (2007).

[24] S. Wycech, F. J. Hartmann, J. Jastrzebski, A. Trzcinska, and T. von Egidy, Nuclear surface studies with antiprotonic x rays, Phys. Rev. C **76**, 034316 (2007).
[25] P. Roberson, T. King, R. Kunselman, J. Miller, R. J. Powers, P. D. Barnes, R. A. Eisenstein, R. B. Sutton, W. C. Lam, C. R. Cox, M. Eckhause, J. R. Kane, A. M. Rushton, W. F. Vulcan, and R. E. Welsh, Strong interaction and mass measurements using antiprotonic atoms, Phys. Rev. C **16**, 1945 (1977).
[26] H. Poth, Compilation of Data from Hadronic Atoms (Fachinformationszentrum Energie, Physik, Mathematik, Karlsruhe, Germany, 1979).
[27] F. J. Hartmann *et al.*, Nucleon density in the nuclear periphery determined with antiprotonic x rays: Calcium isotopes, Phys. Rev. C **65**, 014306 (2001).
[28] B. Kłos *et al.*, Neutron density distributions from antiprotonic ^{208}Pb and ^{209}Bi, Phys. Rev. C **76**, 014311 (2007).
[29] P. Möller, A. J. Sierk, T. Ichikawa, and H. Sagawa, Nuclear ground-state masses and deformations, At. Data Nucl. Data Tables **109-110**, 1 (2016).
[30] H. Poth *et al.*, Study of antiprotonic atoms of light nuclei and isotopes, Nucl. Phys. A **294**, 435 (1978).
[31] J. Cugnon, S. Wycech, J. Jastrzebski, and P. Lubinski, Geometrical effects in antiproton annihilation on nuclei, Phys. Rev. C **63**, 027301 (2001).
[32] M. B. Johnson and G. R. Satchler, Characteristics of local pion-nucleus potentials that are equivalent to Kislinger-type potentials, Ann. Phys. (NY) **248**, 134 (1996).
[33] M. Krell and T. E. O. Ericson, Energy levels and wave functions of pionic atoms, Nucl. Phys. B **11**, 521 (1969).
[34] M. Nuseirat, M. A. K. Lodhi, and W. R. Gibbs, Pion nucleus scattering, Phys. Rev. C **58**, 314 (1998).
[35] M. Alquadi and W. R. Gibbs, Final state interaction in pion production from nuclei, Phys. Rev. C **66**, 064604 (2002).
[36] J. Breitschopf, M. Bauer, H. Clement, M. Cröni, H. Denz, E. Friedman, E. F. Gibson, R. Meier, and G. J. Wagner, Pionic charge exchange on the proton from 40 to 250 MeV reactions, Phys. Lett. B **639**, 424 (2006).
[37] W. B. Kaufmann and W. R. Gibbs, Nuclear medium effects in pion elastic and charge exchange scattering, Phys. Rev. C **28**, 1286 (1983).
[38] D. Ashery, I. Navon, G. Azuleos, H. K. Walter, H. J. Pfeiffer, and F. W. Schlepuütz, True absorption and scattering of pions in nuclei, Phys. Rev. C **23**, 2173 (1981).
[39] W. Macke, II Gol'dman and VD Krivchenkov, Problems in Quantum Mechanics. 275 S. m. 33 Abb. Oxford/London/New York/Paris 1961. Pergamon Press. Preis geb. 50 s, Zeitschrift Angewandte Mathematik und Mechanik **41**, 518 (1961).
[40] E. R. Kinney, J. L. Matthews, P. A. M. Gram, D. W. MacArthur, E. Piasetzky, G. A. Rebka, and D. A. Roberts, Inclusive pion double charge exchange in ^{4}He at intermediate energies, Phys. Rev. C **72**, 044608 (2005).
[41] S. A. Wood, J. L. Matthews, G. A. Rebka, P. A. M. Gram, H. J. Ziock, and D. A. Clark, Inclusive Pion Double Charge Exchange in ^{16}O and ^{40}Ca, Phys. Rev. Lett. **54**, 635 (1985).
[42] M. Duer *et al.* (CLAS Collaboration), Direct Observation of Proton-Neutron Short-Range Correlation Dominance in Heavy Nuclei, Phys. Rev. Lett. **122**, 172502 (2019).
[43] J. Rykebush, W. Cosyn, S. Stevens, C. Casset, and J. Nys, Isospin and proton-to-neutron excess dependence of short-range correlations, Phys. Lett. B **792**, 21 (2019).
[44] E. Pedroni *et al.*, Total cross sections on hydrogen and deuterium for pion energies from 50 to 300 MeV, Nucl. Phys. A **300**, 321 (1978).
[45] W. Cosyn and J. Rykebush, Phase space distribution of nuclear short-range correlations, Phys. Lett. B **820**, 136526 (2021).
[46] N. Sandulescu, P. Schuck, and X. Vinas, Nuclear pairing: Surface or bulk, Phys. Rev. C **71**, 054303 (2005).